

# Deep Learning for Detecting and Early Predicting Chronic Obstructive Pulmonary Disease from Spirogram Time Series: A UK Biobank Study

Shuhao Mei<sup>a,\*</sup>, Yuxi Zhou<sup>a,b,\*</sup>, Jiahao Xu<sup>a</sup>, Yuxuan Wan<sup>a</sup>, Shan Cao<sup>c</sup>, Qinghao Zhao<sup>d</sup>, Shijia Geng<sup>e</sup>, Junqing Xie<sup>f</sup>, Shenda Hong<sup>g,h,\*\*</sup>

<sup>a</sup>Department of Computer Science, Tianjin University of Technology, Tianjin, China

<sup>b</sup>DCST, BNRist, RIIT, Institute of Internet Industry, Tsinghua University, Beijing, China

<sup>c</sup>Department of Biotherapy, The Second Hospital of Tianjin Medical University, Tianjin, China

<sup>d</sup>Department of Cardiology, Peking University People's Hospital, Beijing, China

<sup>e</sup>HeartVoice Medical Technology, Hefei, China

<sup>f</sup>Centre for Statistics in Medicine and NIHR Biomedical Research Centre Oxford, University of Oxford, Oxford, UK

<sup>g</sup>National Institute of Health Data Science, Peking University, Beijing, China

<sup>h</sup>Institute of Medical Technology, Peking University, Beijing, China

## Abstract

Chronic Obstructive Pulmonary Disease (COPD) is a chronic inflammatory lung condition that causes airflow obstruction. The existing methods can only detect patients who already have COPD based on obvious features shown in the spirogram (In this article, the spirogram specifically involves measuring Volume-Flow curve time series). Early prediction of COPD risk is vital for monitoring COPD disease progression, slowing it down, or even preventing its onset. However, these methods fail to early predict an individual's probability of COPD in the future based on subtle features in the spirogram. To address this gap, for the **first time**, we propose DeepSpiro, a method based on deep learning for early prediction of future COPD risk. DeepSpiro consists of four parts. First, we construct Volume-Flow curves guided by Time-Volume instability smoothing (SpiroSmoother) to enhance the stability of the original Volume-Flow curves precisely. Second, we extract critical features from the evolution of varied-length key patches (SpiroEncoder) to capture the key temporal evolution from original high-dimensional dynamic sequences to a unified low-dimensional temporal representation. Third, we explain the model based on temporal attention and heterogeneous feature fusion (SpiroExplainer), which integrates information from heterogeneous data such as spirogram and demographic information. Fourth, we predict the risk of COPD based on the evolution of key patch concavity (SpiroPredictor), enabling accurate prediction of the risk of disease in high-risk patients who are not yet diagnosed, for up to 1, 2, 3, 4, 5 years, and beyond. We conduct experiments on the UK Biobank dataset. Results show that DeepSpiro achieves an AUC value of 0.8328 in the task of detecting COPD. In early prediction tasks, high-risk and low-risk groups show significant differences in the future, with a p-value of <0.001. DeepSpiro can effectively predict the future development trend of the disease. Our code is publicly available at <https://github.com/yudaleng/COPD-Early-Prediction>.

**Keywords:** Chronic Obstructive Pulmonary Disease (COPD), Spirogram, Time Series, Deep Learning

## 1. Introduction

Chronic Obstructive Pulmonary Disease (COPD) is a progressively worsening lung disease that leads to difficulty breathing, limited activity, and a decline in quality of life [9, 40]. As the disease progresses, COPD may also increase the risk of cardiovascular diseases [12] and

even lead to premature death. Therefore, timely and accurate COPD detection is crucial to reduce patient health risks [8]. Previous studies have shown a strong correlation between detecting the disease at an early stage and the success of its treatment. Failing to identify the disease during this crucial period will worsen its severity [10, 39].

Clinical diagnosis often involves identifying COPD patients by determining if the FEV1/FVC ratio is below 70% [20, 22, 23]. Researchers have discovered that the FEV1/FVC ratio method is not always accurate when

\*Contributed equally.

\*\*Corresponding author.

Email address: hongshenda@pku.edu.cn (Shenda Hong)

used with people of different ages [11, 21]. This means that some patients might not get the right diagnosis at the right time, missing out on early and personalized treatment options.

In recent years, researchers have used deep learning technologies [3] to identify COPD characteristics by analyzing the Volume-Flow curve. Diagram 3-A shows the differences between healthy individuals and those with COPD on the Volume-Flow curve. This method helps to overcome the limitations of traditional approaches but cannot effectively predict an individual’s latent risk of developing COPD. Moreover, introducing deep learning technology has resulted in models lacking transparency, making it difficult to gain the trust of medical professionals and patients [19]. Therefore, developing an artificial intelligence interpretable algorithm that can accurately detect patients with COPD and early predict an individual’s latent risk of COPD is crucial for slowing disease progression and preventing patient mortality.

However, most existing methods for COPD risk analysis mainly face the following four challenges:

- In order to determine the degree of airflow obstruction, it is necessary to generate Volume-Flow curves based on the original Time-Volume curves. Nevertheless, current techniques for generating Volume-Flow curves can yield unstable curves, potentially resulting in incorrect predictions by the model.
- The length of the Volume-Flow curve varies among individuals due to differences in exhalation durations. yet, existing techniques commonly handle Volume-Flow curves with varying lengths by either filling in missing values or truncating through downsampling. The former can readily add extraneous noise, whereas the latter could sacrifice important data dependencies.
- Existing deep learning models are still black-box models that can only produce detection outcomes without offering an explainer for those results. Models lacking transparency may find it challenging to gain the trust of medical professionals and patients.
- Currently, existing methods can only detect patients who have already had COPD based on obvious characteristics displayed on the spirogram (In this article, the spirogram specifically involves measuring Volume-Flow curve time series). However, these methods fail to early predict an individ-

ual’s probability of COPD in the future based on changes in the spirogram.

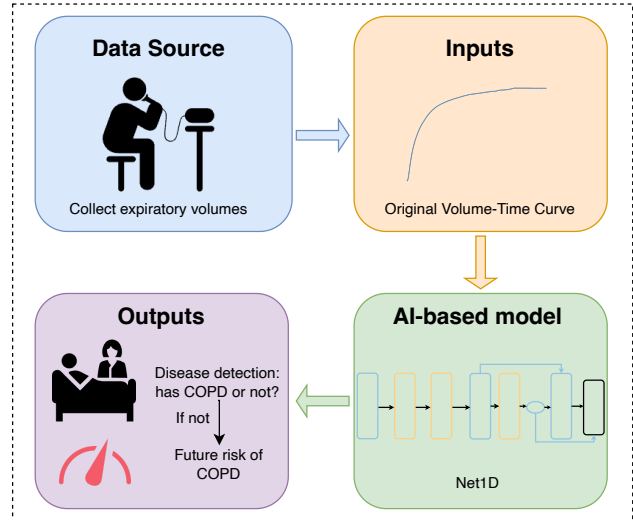


Figure 1: Our method uses the original Time-Volume curve time series collected in hospitals as input. We use neural networks to process the original Time-Volume curve and infer whether an individual has COPD, and if not, predict their risk of COPD in the coming years.

To address the aforementioned challenges, we propose DeepSpiro, a method based on deep learning for early prediction of future COPD risk (Figure 1). Specifically, this paper makes four major contributions:

- We apply a method for constructing Volume-Flow curves guided by Time-Volume instability smoothing (SpiroSmoother), which uses a curve smoothing algorithm to precisely enhance the stability of the Volume-Flow curve while retaining the essential physiological information from the original Volume-Flow data.
- We develop a COPD identification method based on learning from varied-length key patch evolution (SpiroEncoder). This algorithm can dynamically calculate the "key patch" number that is best suited for each time series data patch, thereby unifying the time series representation and extracting key physiological information from the original high-dimensional dynamic sequence into a unified low-dimensional time series representation.
- We propose a method for explaining model based on temporal attention and heterogeneous feature fusion (SpiroExplainer). This method combines the probability of having COPD (Obtained from Module II in figure 2) with demographic data like

age, sex, and probability. This information is then used as input for the model, which outputs a COPD risk assessment and offers an explainer for the model's decisions regarding the individual.

- We develop a method for predicting the risk of COPD based on the evolution of key patch concavity (SpiroPredictor) for the first time. Our method can precisely forecast the probability of disease onset in undiagnosed high-risk patients over the next 1, 2, 3, 4, 5 years, and beyond. Additionally, it can accurately categorize these patients, thereby addressing the current deficiency in early predicting future COPD risk.

## 2. Related Work

In the field of COPD research, the global high incidence and mortality rates highlight the urgency of developing reliable diagnostic methods and early detection strategies. Recent research has focused on three main directions to address this challenge.

### 2.1. Machine Learning and Deep Learning for Detection

The application of machine and deep learning has led to significant advances in the detection of diseases. Here, we summarize key contributions in this field.

Cries Avian et al. [34] make a valuable contribution to the field by suggesting a Convolutional Neural Network (CNN) design for categorizing individuals as smokers or non-smokers, as well as identifying COPD in both healthy subjects and smokers. This classification is based on electronic nose signals. Expanding on the progress made in image-based classification, J Cosentino et al. [3] have made noteworthy contributions to the identification and evaluation of COPD by utilising deep convolutional neural networks to analyse complex lung function graphs and employing machine learning techniques to classify COPD patients into two categories. Similarly, Behnood Dianat et al. [35] investigated the use of deep learning methods to classify lung sounds in patients with connective tissue disease. The uniqueness of this work resides in the creation of an appropriate preprocessing pipeline for removing noise and enhancing the dataset. Additionally, Yonghua Zhuang et al. [5] introduced a ConvGNN model that utilises spectroscopy and combines multiple types of omics data (Such as proteomics and transcriptomics) with disease-specific protein/genetic interactions. This integration allows for accurate classification of COPD and addresses the drawback of relying solely on one

data source. Furthermore, Yanan Wu et al. [6] converted three-dimensional airways and lung fields into multiple two-dimensional snapshots from different perspectives. They employed a deep Convolutional Neural Network (CNN) model to incorporate these snapshots and enhance the accuracy of predicting Chronic Obstructive Pulmonary Disease (COPD) from CT images, demonstrating the benefits of multi-angle image integration techniques.

### 2.2. Machine Learning and Deep Learning for Prediction

Machine learning and deep learning are used to predict disease progression, especially in COPD. Here, we highlight two significant contributions in this field.

Building upon the use of imaging for diagnosing COPD, Konstantin Willer et al. [2] achieved impressive outcomes by employing deep learning models to forecast the five-year survival rate of patients with COPD. The researchers integrated chest X-ray images with clinical data including age, BMI, and FEV1. Although dependent on costly and intricate CT and X-ray machinery, this study offers valuable insights into the diagnosis and prognosis of COPD. Chenzhong Yin et al. [4] improved the diagnosis of COPD by analysing physiological signals and extracting unique features using fractional-order dynamic modelling, which involves studying the complex coupled fractal dynamics. The researchers utilized deep neural networks to forecast the stages of COPD, showcasing the efficacy of this methodology.

### 2.3. Biological and Gene Research

Biological and genetic research has helped us understand COPD better. It has also helped us find genetic markers and potential treatments.

Pooja Sharma et al. [32] use the modular properties of gene networks to detect functionally rich modules in COPD patient samples. They analyzed the modules extracted from COPD samples and identified key genes associated with COVID-19 disease. Zhifa Han et al. [33] demonstrate through MRI studies that a high blood eosinophil count is an independent causal mediator of COPD risk, a decrease in FEV1/FVC, and COPD-related hospitalization. An increase in neutrophil count results from COPD onset or a decrease in FEV1/FVC. This indicates that eosinophils (Rather than neutrophils) could serve as therapeutic targets to prevent the onset and worsening of COPD and the decrease in FEV1/FVC. Yuwei Yang et al. [36] aim to find key genes for the early detection of COPD to avoid the

progression of the disease and to analyze immune cell infiltration in the early and late stages of COPD. This research identified the EXPH5 gene as a marker gene, providing new insights for the clinical diagnosis and drug design of COPD. Yubin Lee et al. [37] proposed a single-cell level mechanism of COPD pathogenesis. They conducted a meta-analysis using three single-cell RNA sequencing datasets of COPD and provided information on toxic compounds that could be potential risk factors for COPD.

### 3. Methods

#### 3.1. Problem Definition

For a COPD dataset  $D = \{X, Y\}$  composed of  $N$  instances, where  $X = \{x_1, x_2, \dots, x_j, \dots, x_N\}$  represents the monitoring data for  $N$  instances, and  $Y = \{y_1, y_2, \dots, y_j, \dots, y_N\}$  represents the COPD disease labels for the  $N$  instances. The disease label for the  $j^{\text{th}}$  instance,  $y_j \in \{0, 1\}$ , with 0 indicating no disease and 1 indicating the presence of disease. The monitoring data  $x_j = \{s_j, d_j, a_j\}$  includes the spirogram data  $s_j$ , demographic information  $d_j = \{dg_j, da_j, ds_j, \dots\}$ , and key concavity information  $a_j = \{a_{j,pef-fef25}, a_{j,fe25-fe50}, a_{j,fe50-fe75}, a_{j,fe75+}\}$ . Here, the spirogram data is a varied-length sequence  $s_j = \{s_{j,1}, s_{j,2}, \dots, s_{j,i}, \dots\}$  representing airflow variation over time during exhalation. In the demographic information,  $dg_j$  denotes sex,  $da_j$  represents age, and  $ds_j$  indicates smoking status. The key patch concavity information includes  $a_{j,pef-fef25}$  for the concavity information between PEF and FEF25,  $a_{j,fe25-fe50}$  for the concavity information between FEF25 and FEF50,  $a_{j,fe50-fe75}$  for the concavity information between FEF50 and FEF75, and  $a_{j,fe75+}$  for the concavity information beyond FEF75.

DeepSpiro takes the monitoring data  $X$  of  $N$  instances as input and produces predicted disease labels  $\hat{Y} = \{\hat{y}_1, \hat{y}_2, \dots, \hat{y}_j, \dots, \hat{y}_N\}$ , explainer  $\hat{E} = \{\hat{e}_1, \hat{e}_2, \dots, \hat{e}_j, \dots, \hat{e}_N\}$ , COPD risk values  $R$  and the risk coefficients contributed by each monitoring input dimension  $R_s, R_{dg}, R_{da}, R_{ds}$ , etc., as well as the probabilities of future disease occurrence for high-risk undiagnosed COPD patients  $F_{copd}, F_{1year}, F_{2year}, F_{3year}, F_{4year}, F_{5year+}, F_{non-copd}$ . Here,  $y_j \in \{0, 1\}$ , where 0 indicates no disease, and 1 indicates the presence of disease.

#### 3.2. Overview

DeepSpiro can be divided into four main modules: 1) SpiroSmoother: constructing Volume-Flow curves guided by Time-Volume instability smoothing: This enhances the stability of key physiological information in the original Volume-Flow data. 2) SpiroEncoder: extracting critical features from the evolution of varied-length key patches: This dynamically identifies "key patches" and unifies the time-series representation, achieving the conversion of key physiological information from high-dimensional to low-dimensional. 3) SpiroExplainer: explaining model based on temporal attention and heterogeneous feature fusion: This combines diagnostic probabilities with demographic information to assess COPD risk and provides an explainer of the model's decisions. 4) SpiroPredictor: predicting the risk of COPD based on the evolution of key patch concavity: This integrates key concavity information to assess COPD risk for various future periods.

Specifically, the original spirogram data is processed with signal enhancement technology to obtain smoothed Volume-Flow data. The smoothed Volume-Flow data is used as input in DeepSpiro for varied-length time series data in order to extract essential physiological information. Subsequently, the model combines the important physiological details and relevant demographic information using temporal attention and heterogeneous feature fusion techniques. This process enables the model to output a COPD risk assessment and provide an explainer for its decisions. By using the COPD risk assessment values and concavity information obtained from the Volume-Flow signals in the feature fusion model, we can make precise predictions about the probability of future disease in high-risk patients who have not yet received a diagnosis.

#### 3.3. SpiroSmoother: Constructing Volume-Flow Curves Guided by Time-Volume Instability Smoothing

The current state-of-the-art (SOTA) method for detecting COPD from the Volume-Flow curve using deep learning has been proposed by J. Cosentino et al. [3]. This method involves converting original Time-Volume curves into Volume-Flow curves, which can result in instability in the curves (As shown in the red section of figure 3-C). Extensive experimental validation has been demonstrated that these instabilities can impact the final risk assessment for COPD patients. To address this, we employ SpiroSmoother. This approach precisely enhances the stability of the original Volume-Flow curves while preserving key physiological signals within the original Volume-Flow data.

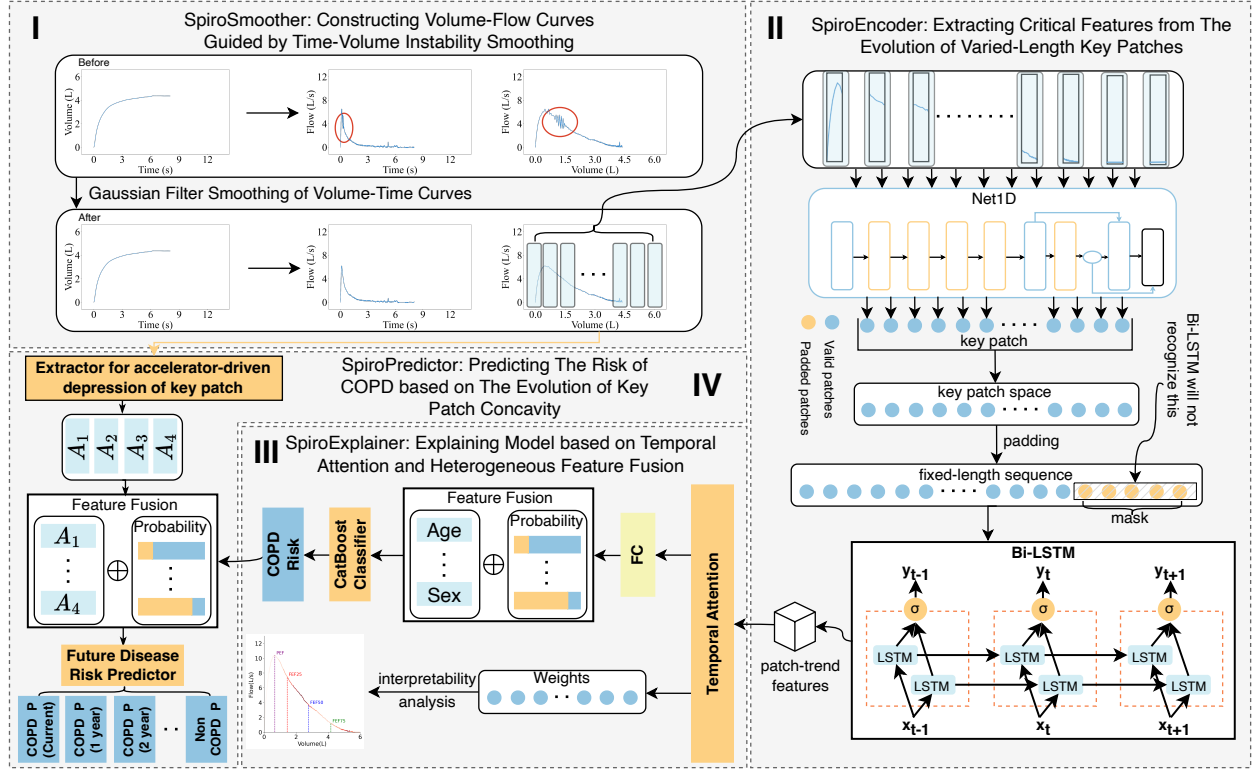


Figure 2: Framework overview. It is divided into four modules. In the first module, we process the varied-length original volume curve and convert it into a smoothed Volume-Flow curve. In the second module, we extract features from the varied-length Volume-Flow curve. In the third module, combined with demographic information, we output the COPD detection results and model explainer. In the fourth module, based on concavity information, we output the risk values for COPD at different future periods.

As shown in figure 3-C, we observe instability when converting the Time-Volume curve into a Time-Flow curve. Therefore, we believe that smoothing the original Time-Volume curve could help enhance the stability of both the Time-Flow curve and the Volume-Flow curve.

Gaussian filtering is employed to implement instability smoothing guidance for the original Time-Volume curves. This method achieves smoothing by taking a weighted average of the areas around the data points, where the weight of each data point is determined by a Gaussian function. For a given data point  $x_i$  its smoothed value  $y_i$  can be defined as:

$$y_i = \frac{\sum_{j=-k}^k x_{i+j} \cdot g(j)}{\sum_{j=-k}^k g(j)} \quad (1)$$

In this formula,  $g(j)$  represents the Gaussian function,  $k$  is the filter's window size, and  $x_{i+j}$  represents the original data point and its adjacent points. The formula calculates the weighted average of data points around  $x_i$ , using weights derived from the Gaussian function  $g(j)$ .

This function is centered at  $x_i$ , and its standard deviation determines both the range and the degree of smoothing. Through this method, Gaussian filtering effectively smooths the data while preserving important feature information.

To convert the smoothed Time-Volume curve into a Volume-Flow curve, we utilize the finite difference method to approximate the first derivative of the volume data with respect to time. Simply put, it involves calculating the volume change rate at consecutive time points to obtain corresponding flow data. The flow  $Q(t)$  can be obtained by calculating the derivative of volume  $V(t)$  with respect to time  $t$ , where flow  $Q(t)$  is defined as:

$$Q(t) \approx \frac{V(t + \Delta t) - V(t)}{\Delta t} \quad (2)$$

Where  $V(t)$  represents a set of Time-Volume curve data,  $\Delta t$  is the time interval between two adjacent time points, and  $t$  denotes the time points.

We linearly interpolate the calculated flow data to ensure that the Time-Flow curve is consistent with the original Time-Volume curve in terms of time data. In

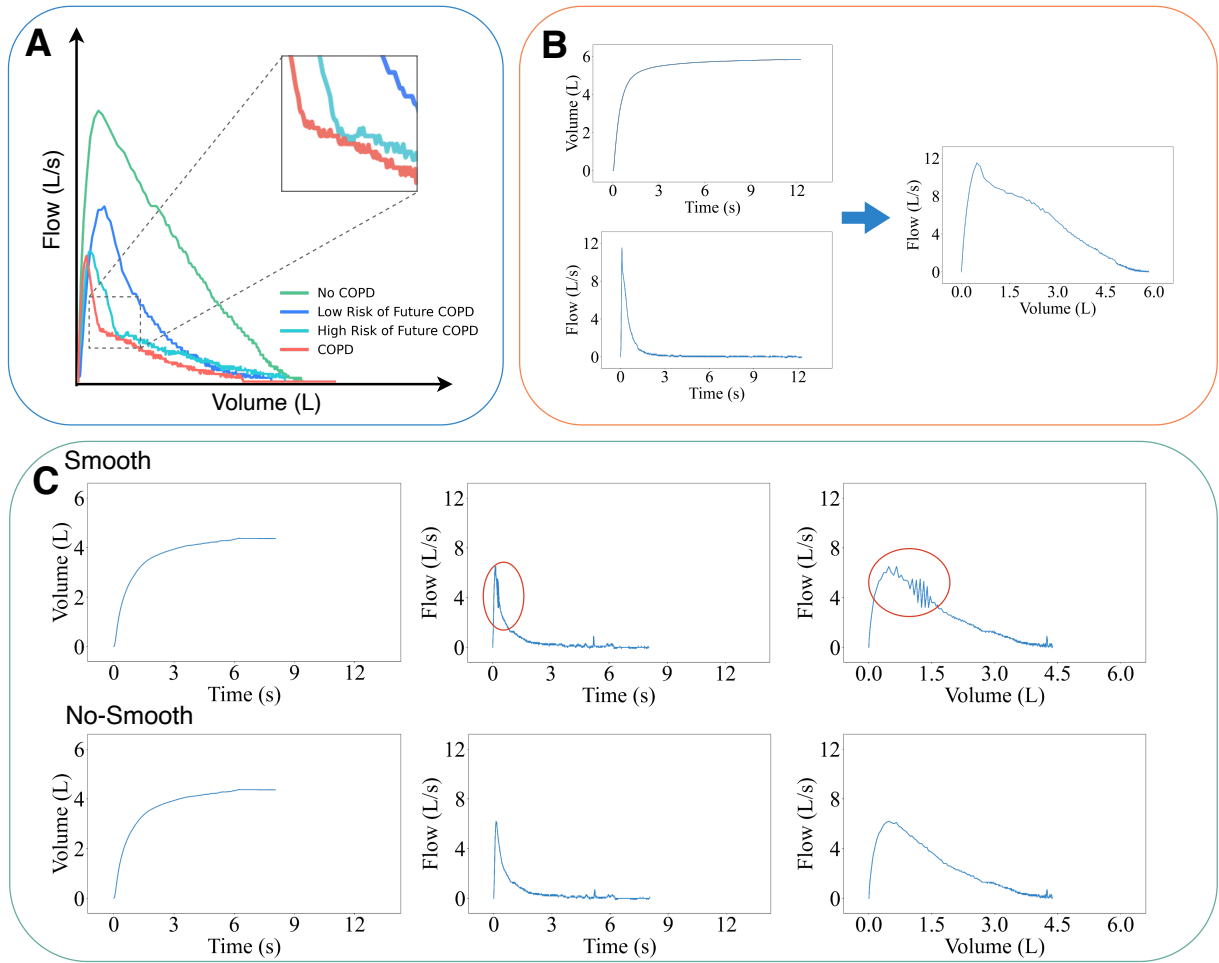


Figure 3: For figure A, Example of a Volume-Flow diagram, where the dotted line shows the schematic of a normal individual and the solid line shows the schematic of a patient with COPD. Key points on these curves are labeled to indicate peak expiratory flow rate ( $PEF$ ) and forced expiratory flow rates at 25%, 50%, and 75% of the forced vital capacity ( $FEF_{25}$ ,  $FEF_{50}$ ,  $FEF_{75}$ , respectively). For figure B, Diagram illustrating the conversion of the original Time-Volume curve. To obtain the degree of airflow limitation, we need to use finite difference methods on the original Time-Volume curve. For figure C, smoothing comparison, the original curve shows fluctuations in some areas (Circled in red) when converting to Time-Flow and Volume-Flow curves. After smoothing, the curves in the same positions become more stable.

this way, we can construct the Volume-Flow curves using the Time-Flow curves and the Time-Volume curves.

As shown in figure 3-C, the Time-Flow curve and the Volume-Flow curve have been constructed using the Time-Volume instability smoothing guidance technique and have effectively eliminated the original fluctuations, significantly enhancing the data's stability. In subsequent experiments, we have used these stable Volume-Flow curves to replace the original data for model training. Experimental results have confirmed that the curves processed through instability smoothing guidance demonstrate superior performance in risk assess-

ment.

### 3.4. SpiroEncoder: Extracting Critical Features from The Evolution of Varied-Length Key Patches

Existing methods for modeling varied-length time series data generally use missing value imputation or downsampling truncation. The former introduces external noise, while the latter will likely lose meaningful data dependencies. We aim to preserve the key signals of the original data and adapt them to model input. To this end, we propose SpiroEncoder.

First, we need to reconstruct the original data. We have adopted an adaptive temporal decomposition

method, which dynamically calculates the most suitable "key patches" count for each time series patch, accurately capturing the key Volume-Flow information within each time patch. By introducing the hyperparameter  $k$ , we can calculate the number of key patches based on the ratio of the sequence length to  $k$ , ensuring that each patch contains enough information for subsequent analysis. For a given length of time series  $L$ , the number of key patches  $S$  can be defined as:

$$S = \left\lceil \frac{L}{k} \right\rceil \quad (3)$$

Where  $\lceil \cdot \rceil$  represents the ceiling function, ensuring that meaningful data dependencies are not lost even when  $L$  is not divisible by  $k$ .

We can obtain the number of key patches for each sequence using the abovementioned method. Thus, we can divide each sequence into several key patches. We feed all the key patches into the Net1D network [7] to extract the spatial features between the patches and the temporal features within each patch. The Net1D network extracts spatial features for us. We must compress the high-dimensional spirogram space into the same low-dimensional key patch to adapt these features for our subsequent modules.

First, we determine the length of the most extended sequence in the dataset and use this length along with the preset hyperparameter  $k$ . Calculate the number of key patches all sequences should have, thereby normalizing the temporal representation of the data. For the longest sequence length  $L_{\max}$  in the dataset, the maximum number of patches is defined as:

$$N_{\max} = \left\lceil \frac{L_{\max}}{k} \right\rceil \quad (4)$$

We perform encoding for the key features of each sequence. This encoding marks the key patches and records them as a mask. For each sequence, we create a mask vector. Parts of the vector where key patches exist are masked as 1, and parts extending from the end of the existing key patches to the maximum number of patches are masked as 0.

We construct a zero tensor  $O \in \mathbb{R}^{N \times S \times C}$ , where  $N$  represents the number of samples,  $S$  represents the number of key patches, and  $C$  represents the number of output channels. Subsequently, we selectively apply these encodings to the zero tensor  $O$  using the mask vector. For each sample, the mask vector indicates where to insert the features of key patches. Specifically, if the mask vector is one at a certain position, then we insert the encoding at the corresponding position in the zero tensor

$O$ ; if the mask vector is 0 at a position, the zero tensor remains unprocessed at that position (This part also constitutes the padding of 0s for the sequence). Thus, the zero tensor  $O$  transforms into a fixed-length sequence containing encoding information, and we refer to the transformed zero tensor  $O$  as the feature tensor of key patches  $O$ . For each sample  $i$  and its key patches  $j$ , we use the mask vector  $M_{i,j}$  to decide whether to apply encoding.  $O_{i,j,:}$  can be defined as:

$$O_{i,j,:} = M_{i,j} \cdot E_{i,j,:} \quad (5)$$

where the features extracted by Net1D for each key patch are  $E_{i,j,:} \in \mathbb{R}^C$

Because the process of constructing the key patch feature tensor  $O$  involves padding with zeros, this padded information may introduce unnecessary noise when captured by the Bidirectional Long Short-Term Memory Network (Bi-LSTM). To address this, we aim to effectively ignore this portion of padded information before entering the Long Short-Term Memory Network.

First, we calculate the effective length  $Length_i$  for each sequence, which is the number of valid key patches in the sequence  $i$ . The effective length  $Length_i$  can be defined as:

$$Length_i = \sum_{j=1}^S M_{i,j} \quad (6)$$

Then, we create a new tensor  $P \in \mathbb{R}^{T \times C}$ , where  $T = \sum_{i=1}^N Length_i$ , that is, the sum of the effective lengths of all sequences, and  $C$  is the number of output channels. Following the sequence order, we copy the features of valid key patches from the key patch feature tensor  $O$  into the tensor  $P$ . After the above steps, the tensor  $P$  contains only valid key patch features.

After the tensor  $P$  enters the Bidirectional Long Short-Term Memory network (Bi-LSTM) [13], the evolutionary relationship between key patches is obtained.

### 3.5. SpiroExplainer: Explaining Model based on Temporal Attention and Heterogeneous Feature Fusion

Existing deep learning models still function as black boxes, capable only of producing diagnostic outcomes without offering an explainer for those results. In order to establish credibility with medical professionals and patients, the model must offer a decision-making process that is more open and easily understood by both parties. Therefore, through the dynamic temporal attention integration method, we accurately highlight the time patches crucial for model predictions using a

method for explaining model based on temporal attention and heterogeneous feature fusion.

Data enters the first linear transformation layer as it passes through the temporal attention layer. This layer provides an initial feature representation for each time step, which is specifically manifested as:

$$X' = W_1 X + b_1 \quad (7)$$

Here,  $W_1$  and  $b_1$  are the weight and bias of the linear layer, respectively.

To perform a nonlinear transformation, We follow up by applying the Swish activation function to the linearly transformed data  $X'$ . This helps to improve the model's ability to capture complex features. After that, we apply a bilinear transformation to the activated data  $X''$  by using a bilinear weight matrix. This is specifically represented as:

$$X''' = X'' W_{\text{bil}} \quad (8)$$

where  $W_{\text{bil}}$  is the bilinear weight matrix.

After passing through the bilinear transformation, the data  $X'''$  goes through another linear layer to calculate the attention scores  $S$  for each time step. Finally, the  $S$  scores are normalized using the *softmax* function to obtain the temporal attention weights.

We combine the temporal attention information with the smoothed Time-Volume curve data. The decision-making process within the deep neural network model can be transformed into visualized graphs. The graphs provide a clear representation of the specific data regions that the model prioritizes when making decisions, thereby improving the transparency of the model and bolstering the credibility of its decision-making process.

Research indicates that there is a significant correlation between smoking, age, and other demographic information with COPD. Therefore, we aim to incorporate some demographic information to enhance the effectiveness of our model. For this purpose, after passing through the temporal attention layer, we first conduct an initial COPD assessment through a fully connected layer, resulting in  $\hat{P} = \{\hat{p}^1, \hat{p}^2, \dots, \hat{p}^j, \dots, \hat{p}^N\}$ , where  $\hat{P}$  represents a series of COPD assessment values for the samples, with  $\hat{p}^j \in [0, 1]$  denoting the assessment value for the  $j$ -th sample. Up to this point, the unstructured varied-length Volume-Flow curve data has been transformed into structured COPD assessment values. We fuse the COPD assessment values  $F_{\text{time}}$  with traditional demographic  $F_{\text{struct}}$  and other structured information to obtain  $F_{\text{fusion}}$ . The fusion operation can be represented as:

$$F_{\text{fusion}} = F_{\text{time}} \oplus F_{\text{struct}} \quad (9)$$

By utilizing the Gradient Boosting framework (Catboost) to process the fused features  $F_{\text{fusion}}$ , we predict the risk of COPD. The COPD risk assessment obtained in this manner will outperform the assessment results derived solely from unstructured varied-length Volume-Flow curve data.

### 3.6. SpiroPredictor: Predicting The Risk of COPD based on The Evolution of Key Patch Concavity

In future risk prediction tasks, we used the degree of concavity in individual Volume-Flow graphs as one of the features for prediction. As shown in figure 3-A, high-risk individuals and COPD patients exhibit more significant concavity, while low-risk individuals exhibit fewer concavity than high-risk individuals and COPD patients. The following will provide a detailed explanation of how this feature of concavity is extracted.

We categorize the stages of a patient's illness into seven classes: already ill, becoming ill within 1 year, within 2 years, within 3 years, within 4 years, within 5 years or later, and not ill. We also convert the Volume-Flow curve into a flow acceleration curve. Assuming the Volume-Flow curve is represented by the function  $V(t)$ , where  $V$  is the volume (L) and  $t$  is time (S). The flow, being the first derivative of volume with respect to time, can be expressed as  $Q(t) = \frac{dV}{dt}$ . The acceleration of flow, which is the first derivative of flow with respect to time, can be represented as  $A(t) = \frac{d^2V}{dt^2}$ .

The key patch concavity information in the Volume-Flow curve can be obtained through the average acceleration of key patches. Therefore, we need to calculate the average acceleration between  $PEF$  (Peak Expiratory Flow) and  $FEF_{25}$  (25% Expiratory Flow), the average acceleration among  $FEF_{25}$ ,  $FEF_{50}$  (50% Expiratory Flow), and  $FEF_{75}$  (75% Expiratory Flow), as well as the average acceleration after  $FEF_{75}$ . Taking the average acceleration between  $PEF$  and  $FEF_{25}$  as an example, assuming the time point corresponds to  $PEF$  is  $t_{PEF}$  and the time point corresponding to  $FEF_{25}$  is  $t_{25}$ , then the average acceleration between  $PEF$  and  $FEF_{25}$  can be expressed as:

$$A_{PEF-FEF25} = \frac{1}{t_{25} - t_{PEF}} \int_{t_{PEF}}^{t_{25}} A(t) dt \quad (10)$$

$A_{PEF-FEF25}$  represents the concavity information between  $PEF$  and  $FEF_{25}$ , and is also one of the key patch concavity information.

We fuse the COPD risk identified by the explainer method of the model based on temporal attention and heterogeneous feature fusion with the key concavity information of the Volume-Flow curve and input this com-



bin data into a future disease risk predictor for assessing future risk. Our future disease risk predictor can be classifiers like Catboost [17], Xgboost [16], Random Forest [18], etc. The model, having been obtained in this way, accurately predicts the probability of illness in the next 1, 2, 3, 4, 5 years, and beyond for high-risk patients who have not yet been diagnosed.

## 4. Experiments and Results

### 4.1. Experimental Setup

#### 4.1.1. Dataset and Preprocessing

The data used in our study was obtained from the UK Biobank. We specifically focused on information from 453,558 patients who underwent their initial pulmonary function test (The test outputs the Time-Volume time-series curve). In order to ensure the quality and usability of the data, we perform thorough preprocessing to eliminate any incomplete or unreliable data.

The original Time-Volume (Expiratory volumes over a period of time) measurements are extracted from UK Biobank field 3066, which contains expiratory volumes recorded every 10 milliseconds in milliliters. The Time-Volume measurements are used from each participant’s first visit. To ensure the Time-Volume data are valid, we consult UK Biobank field 3061; if the value in field 3061 is either 0 or 32, the expiration is considered valid. If multiple valid expirations are available, we choose the first one in sequence. To control the quality of the expirations, we review the UK Biobank fields 3062 (FVC), 3063 (FEV1), and 3064 (PEF); if any of these are in the top or bottom 0.5% of the observed values, any expiratory data will discard from that patient. The original expiratory volume measurements are converted from milliliters to liters, and the corresponding flow curves are calculated by approximating the first derivative with respect to time using finite differences. As shown in figure 3-B, the Time-Flow and Time-Volume curves combine to generate a one-dimensional Volume-Flow curve time series.

We refer to the labeling methods in Justin Cosentino et al.’s research [3]. Specifically, the labels are generated by combining information from various sources in the UK Biobank. We use a binary COPD label that is determined through self-reporting, hospital admissions, and primary care reports to train DeepSpiro. Self-reported COPD status is derived from codes 1112, 1113, and 1472 in the UK Biobank field 20002. Hospital-reported COPD status comes from codes like J430 and others in the UK Biobank field 41270, and codes like 4920 and others in field 41271. The COPD status

from primary care reports is required using TRUD to map the UK Biobank’s gp-clinical to read codes from UK Biobank field 42040, with mapped fields including codes like J430, among others. For specific extraction of field codes, please refer to the table 4.1.1. In addition, death information is used in subsequent analyses. Death information is recorded in UK Biobank field 40000. If any value is present in this field, we consider the patient to have died.

Table 1: The following table lists the required fields and corresponding codes during label extraction.

| Field Id | Code   | Type            |
|----------|--|-----------------|
| 20002    | 1112,1113,1472                                     | Self Report     |
| 41270    | J430,J431,J432,J438<br>439J,J440,J441,J448<br>J449 | Hospitalization |
| 41271    | 4920,4928,4929,496X                                | Hospitalization |
| 42040    | J430,J431,J432,J438<br>439J,J440,J441,J448<br>J449 | Primary Care    |

A code suffixed with ‘X’ stands for any code starting with the figures preceding the X.

After completing the necessary data processing, the dataset now comprises a total of 348,039 participants. The dataset is partitioned into training and test sets in an 8:2 ratio. The training set comprises 278,431 participants, while the test set comprises 69,608 participants.

#### 4.1.2. Evaluations

To evaluate the performance of this method, we used a validation set to calculate the model’s AUROC (Area Under the Receiver Operating Characteristic curve), AUPRC (Area Under the Precision-Recall Curve), and F1 scores.

**AUROC:** The area under the receiver operating characteristic curve (AUROC) is a widely used metric for evaluating the performance of classification models, especially in binary classification problems. It is calculated by varying the classification threshold to determine the true positive rate ( $TPR = \frac{TP}{TP+FN}$ ) and the false positive rate ( $FPR = \frac{FP}{FP+TN}$ ). The ROC curve shows the relationship between the true positive rate and the false positive rate. The value of AUROC is the area under the ROC curve, which can be approximated as  $AUROC = \int_0^1 R(F) dF$ , where  $F$  represents the false positive rate and  $R(F)$  is the corresponding true positive rate. Numerical methods generally estimate the FPR values  $f_1, f_2, \dots, f_n$  and the corresponding TPR values  $t_1, t_2, \dots, t_n$ . The trapezoidal area approximation of the AUROC is:  $AUROC \approx \sum_{i=1}^{n-1} \frac{(f_{i+1}-f_i) \times (t_i+t_{i+1})}{2}$ .

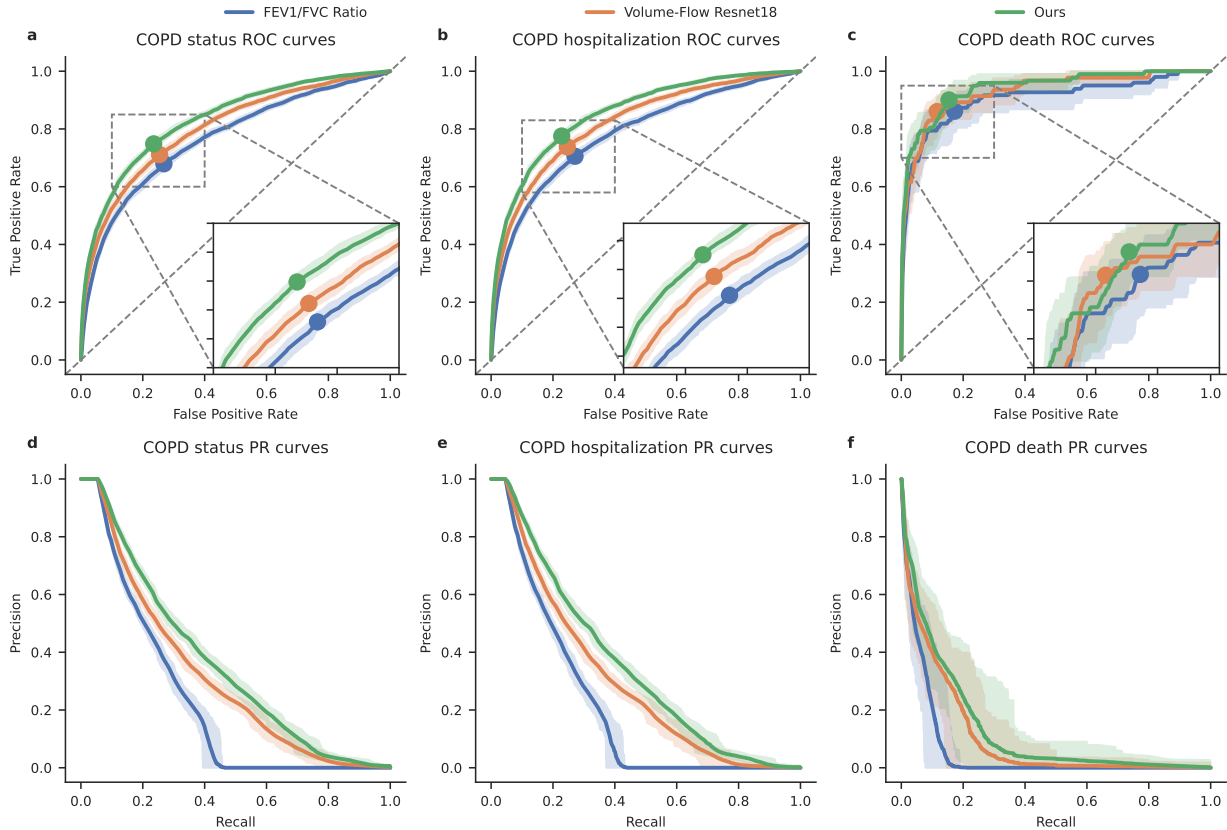


Figure 4: Evaluation comparison. The blue line represents the method of detecting COPD using the FEV1/FVC ratio. A ratio of less than 0.7 is considered as COPD. The orange line represents the method of detecting COPD using the ResNet18 model. The green line represents the method using DeepSpiro to detect COPD. We compared the AUROC and AUPRC of the three methods on the full dataset, the hospitalization dataset (Only includes individuals registered as inpatients), and the death dataset (Only includes individuals registered as deceased).

**AUPRC:** The area under the precision-recall curve (AUPRC) is a commonly used metric to evaluate models for classification problems. The PR curve is derived by varying the classification threshold to calculate precision ( $precision = \frac{TP}{TP+FP}$ ) and recall ( $recall = TPR = \frac{TP}{TP+FN}$ ). It can be approximated as  $\int P(r) dR(r)$ , where  $P(r)$  represents precision,  $R(r)$  denotes recall, and  $r$  represents the decision threshold.

**F1 Score:** The F1 score is a crucial metric for evaluating the accuracy of a model. It is the harmonic mean of precision and recall ( $F1 = 2 \times \frac{precision \times recall}{precision + recall}$ ), providing a single metric that considers both the accuracy and completeness of the model.

These metrics collectively help us comprehensively assess the model’s performance across different aspects. In this experiment, the AUROC, AUPRC, and F1 scores are calculated using functions from the scikit-learn library and code from Justin Cosentino et al. [3].

#### 4.1.3. Compared Methods

To assess the effectiveness of DeepSpiro, we compared it against several baseline methods, including:

- **FEV1/FVC ratio:** The FEV1/FVC ratio is the GOLD standard in clinical practice for determining whether an individual has COPD. If an individual’s ratio is less than 70%, they are considered to have COPD. Therefore, this method will also be used as our baseline.
- **ResNet18 (Nature Genetics):** The ResNet18 convolutional neural network (CNN) is capable of efficiently learning features from large-scale datasets. In a paper published in Nature Genetics, Justin Cosentino et al. utilized this model for the task of COPD detection [3]. Therefore, we also adopt this model as the primary baseline.

Table 2: Evaluation comparison table. This table presents the AUROC, AUPRC, and F1 scores for detecting COPD using four different methods: the FEV1/FVC method, the ResNet18 model, DeepSpiro trained on unsmoothed curves, and DeepSpiro trained on smoothed curves.

| Category        | Method                   | AUROC         | AUPRC         | F1-Score      |
|-----------------|--------------------------|---------------|---------------|---------------|
| All             | FEV1/FVC [41]            | 0.7771        | 0.2266        | 0.3143        |
|                 | Volume-Flow ResNet18 [3] | 0.8212        | 0.3446        | 0.3814        |
|                 | DeepSpiro (non-smooth)   | 0.8315        | 0.3537        | 0.3913        |
|                 | DeepSpiro                | <b>0.8328</b> | <b>0.3570</b> | <b>0.3950</b> |
| Hospitalization | FEV1/FVC [41]            | 0.7925        | 0.2079        | 0.3024        |
|                 | Volume-Flow ResNet18 [3] | 0.8382        | 0.3247        | 0.3703        |
|                 | DeepSpiro (non-smooth)   | 0.8527        | 0.3453        | 0.3871        |
|                 | DeepSpiro                | <b>0.8538</b> | <b>0.3490</b> | <b>0.3900</b> |
| Death           | FEV1/FVC [41]            | 0.9242        | 0.0393        | 0.1206        |
|                 | Volume-Flow ResNet18 [3] | 0.9374        | 0.0887        | 0.2026        |
|                 | DeepSpiro (non-smooth)   | <b>0.9419</b> | 0.1129        | 0.2211        |
|                 | DeepSpiro                | <b>0.9419</b> | <b>0.1165</b> | <b>0.2304</b> |

#### 4.2. Model Detection and Prediction Performance

In this study, we aim to detect COPD and validate DeepSpiro superiority by comparing it to a ResNet18 baseline model. Justin Cosentino et al. proposed this baseline model in a paper published in Nature Genetics [3]. It was trained and evaluated on the UK Biobank dataset, with evaluation metrics including AUROC, AUPRC, and F1-score. To ensure a fair comparison, we used the same dataset and evaluation criteria. In the COPD detection task, DeepSpiro achieved an AUROC of 83.28%, an AUPRC of 35.70%, and an F1-score of 39.50% as shown in figure 4. DeepSpiro outperformed the baseline model in these metrics by 1.16%, 1.24%, and 1.36%, respectively.

Table 2 presents a comparison of different metrics prior to and following signal enhancement. Based on the experimental findings, our signal enhancement technique effectively improves the stability of the Volume-Flow curve without compromising the essential physiological information of the original Volume-Flow data. This enhancement greatly aids in evaluating patients with COPD.

DeepSpiro emphasizes data integrity and the preservation of key information, in contrast to the Volume-Flow ResNet18 method (Baseline model). Based on the experimental findings, DeepSpiro betters the Volume-Flow ResNet18 method in all categories, as evidenced by higher values of key metrics such as AUROC, AUPRC, and F1-score.

In terms of parameters, DeepSpiro also performs exceptionally well. In order to demonstrate the specific advantages of our proposed DeepSpiro with respect to certain parameters, a comparative study is carried out

Table 3: Comparison of model parameters and floating point operations.

| Model                    | # of Params | FLOPs     |
|--------------------------|-------------|-----------|
| Volume-Flow ResNet18 [3] | 3,918,560   | 3,929,184 |
| DeepSpiro                | 125,210     | 124,800   |

between DeepSpiro and the Volume-Flow ResNet18 model. Specifically, Pytorch is used to build both models and utilize the thop library to calculate both models’ parameter count and floating-point operations. The calculation results are shown in table 3. The results indicate that DeepSpiro’s parameter count and floating-point operations are significantly lower than those of the Volume-Flow ResNet18 model.

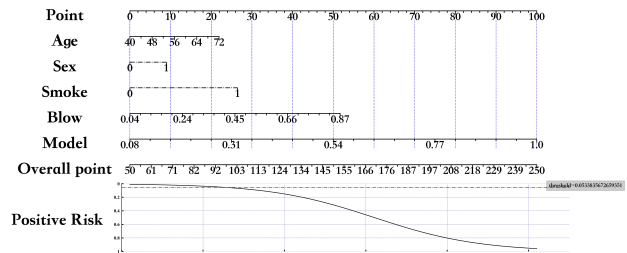


Figure 5: The nomogram of COPD detection.

By leveraging demographic information, the model can gain a more comprehensive understanding of the patient’s background [14], and on this basis, improve its prediction accuracy. Additionally, incorporating FEV1/FVC, the gold standard for COPD diagnosis, into

the model can enhance the model’s capability in diagnosing COPD. To more comprehensively reflect the improvement in the model’s diagnostic capability by demographic information and the FEV1/FVC diagnostic gold standard [27, 25, 26], we concatenate the probabilities outputted by module II (Figure 2-II), demographic information, and the FEV1/FVC diagnostic gold standard into a new vector and input it into a logistic regression model. Figure 5 is a nomogram [29], from which we can intuitively see that the added demographic information and the FEV1/FVC diagnostic gold standard enhance the model’s diagnostic accuracy. Therefore, the model explainer method based on temporal attention and heterogeneous feature fusion has a promotive effect on the diagnosis of COPD.

In summary, traditional pulmonary function assessment indicators cannot fully reflect the disease’s complexity and patients’ overall health status. As shown in table 2, DeepSpiro is more advanced than traditional pulmonary function assessment indicators and the Volume-Flow ResNet18 model.

#### 4.3. Future Risk Prediction Analysis

As shown in figure 3-A, the comparison of concavity degree is displayed for healthy individuals, high-risk group, low-risk group, and COPD patients. By leveraging the information on concavity in the Volume-Flow curve and integrating it with heterogeneous features for the risk of COPD, the model can capture the characteristics of future COPD onset and accurately classify different onset times. Figure 6 includes the distribution probabilities of 7 categories, where the line graph represents the degree of concavity (The larger the absolute value, the lesser the degree of concavity) in the Volume-Flow curve after  $FEF_{25}-FEF_{50}$ ,  $FEF_{50}-FEF_{75}$ , and beyond  $FEF_{75}$ . The  $PEF-FEF_{25}$  region is the most effective area for distinguishing COPD patients. As shown in figure 6, non-COPD patients have the smallest degree of concavity, while COPD patients and those at different future stages of COPD have a greater degree of concavity than non-COPD patients. Notably, as the time to diagnosis progresses, the degree of concavity in  $FEF_{25}-FEF_{50}$  and  $FEF_{50}-FEF_{75}$  decreases, indicating a more saturated curve.

Figure 7 includes the future disease risk of high-risk and low-risk populations. The model predicts individuals as a high-risk group for those identified as at risk of disease and as a low-risk group for those predicted not to have the disease. We plotted the changes in disease risk for both groups as curves, showing the proportion diagnosed with COPD over time. The X-axis

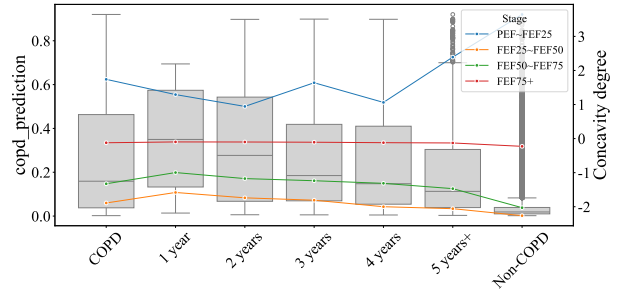


Figure 6: The degree of concavity in different future periods.

represents the time elapsed since the pulmonary function test, and the Y-axis represents the proportion of patients diagnosed with COPD at a specific timestamp within the population, i.e., the risk of disease. From the figure, it can be seen that from the time of the pulmonary function test, the disease risk for the model-predicted high-risk group shows an exponential increase over time, while the disease risk for the low-risk group remains near zero, essentially unchanged with a slight and weak increase. High-risk and low-risk groups also exhibit significant differences, with a p-value of  $p < 0.001$ .

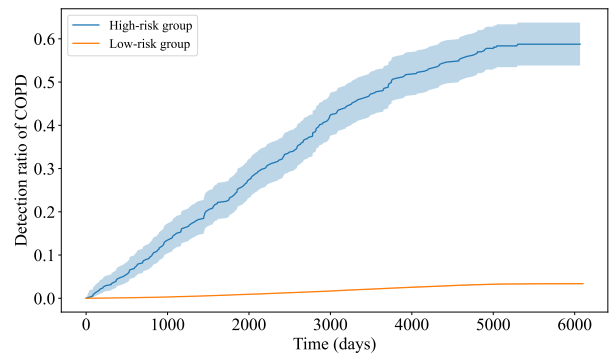


Figure 7: Survival analysis for high and low-risk group.

From the predictive distribution probabilities over future times and the future disease risk scenarios for high-risk and low-risk populations, it can be seen that DeepSpiro can effectively predict the future development trends of the disease, thereby providing better treatment and management plans for patients.

#### 4.4. Result of Subgroup Analysis

To further explore the diagnostic accuracy of the model across different subsets of the population, subgroup analyses for various age groups, sex, and smoking statuses are conducted.

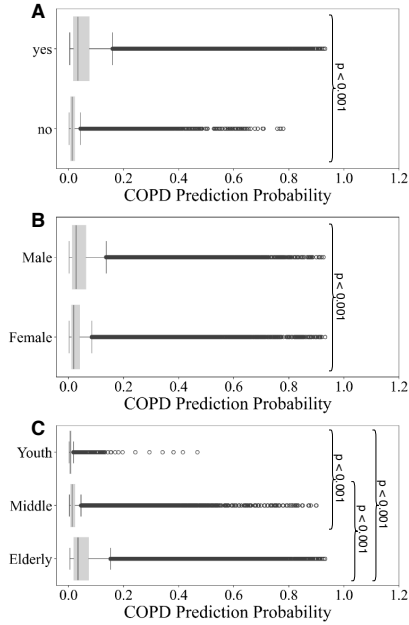


Figure 8: Subgroup analysis. Group A is the subgroup analysis for smoking, Group B is the subgroup analysis by sex, and Group C is the subgroup analysis by age.

The subgroup analysis results for smokers illustrate the model’s application scenarios. Among patients with COPD, the prevalence rate in smokers is higher than in non-smokers [38]. For our model, as shown in Group A of figure 8, the prediction probability for smokers is higher than for non-smokers, and the prediction range for smokers is also wider than that for the non-smoking population. This is consistent with clinical significance. Regarding the p-value, the model demonstrates a strong discriminative ability between the two groups.

The subgroup analysis results for sex showcase the model’s application scenarios. The 2018 China Adult Lung Health Study, which has surveyed 50,991 individuals across ten provinces and cities, has shown that the incidence rate among men is higher than that among women, with men at 11.9% and women at 5.4%. For our model, as shown in Group B of figure 8, the prediction probability for men is higher than for women, and the prediction range for men is also greater than that for women. This aligns with clinical significance. Regarding the p-value, the model demonstrates a strong discriminative ability between the two groups.

Age is a significant factor influencing the development of COPD. Typically, the high-incidence age range for COPD is between 45-80 years. Within this age range, patients’ lung functions tend to decline gradually. Particularly after age 45, the trend of declining

Table 4: Comparison of subgroup evaluations. This table shows the performance of different methods in detecting COPD across various subgroup analyses. These methods include the FEV1/FVC method, the ResNet18 model, and DeepSpiro trained on smoothed Volume-Flow curves.

| Group | Class   | Model         | AUROC         |
|-------|---------|---------------|---------------|
| Sex   | Male    | FEV1/FVC [41] | 0.7719        |
|       |         | ResNet18 [3]  | 0.8166        |
|       |         | DeepSpiro     | <b>0.8335</b> |
|       | Female  | FEV1/FVC [41] | 0.7629        |
|       |         | ResNet18 [3]  | 0.8196        |
|       |         | DeepSpiro     | <b>0.8329</b> |
| Smoke | Yes     | FEV1/FVC [41] | 0.7774        |
|       |         | ResNet18 [3]  | 0.8223        |
|       |         | DeepSpiro     | <b>0.8266</b> |
|       | No      | FEV1/FVC [41] | 0.6857        |
|       |         | ResNet18 [3]  | 0.7428        |
|       |         | DeepSpiro     | <b>0.7620</b> |
| Age   | Youth   | FEV1/FVC [41] | 0.6960        |
|       |         | ResNet18 [3]  | 0.7344        |
|       |         | DeepSpiro     | <b>0.7634</b> |
|       | Middle  | FEV1/FVC [41] | 0.7325        |
|       |         | ResNet18 [3]  | 0.7779        |
|       |         | DeepSpiro     | <b>0.8022</b> |
|       | Elderly | FEV1/FVC [41] | 0.7622        |
|       |         | ResNet18 [3]  | 0.8024        |
|       |         | DeepSpiro     | <b>0.8210</b> |

Note: ResNet18 in the table refers to Volume-Flow ResNet18.

lung function becomes more apparent. After reaching 80 years, lung function further declines, and patients’ immune systems weaken, making them relatively more susceptible to diseases. Therefore, prevention and early identification of COPD are especially important for this age group. We divide patients into Youth (18-44), Middle (45-55), and Elderly (55 and above) for subgroup analysis, as shown in Group C of figure 8. The results indicate that DeepSpiro’s prediction probability for smokers is higher than for non-smokers, and the prediction range for smokers is also larger than for the non-smoking population, consistent with clinical significance. Regarding the p-value, the model shows strong discriminative ability between the two groups.

Additionally, we compare the AUROC of DeepSpiro, the Volume-Flow ResNet18 model, and the FEV1/FVC metric across different subgroups, as shown in table 4. Across all subgroups, DeepSpiro’s AUROC is the highest, demonstrating DeepSpiro’s applicability in different

subgroups.

#### 4.5. Result of SHAP Analysis

To further analyze whether the model’s predictions hold clinical significance, we conduct a SHAP analysis [15].

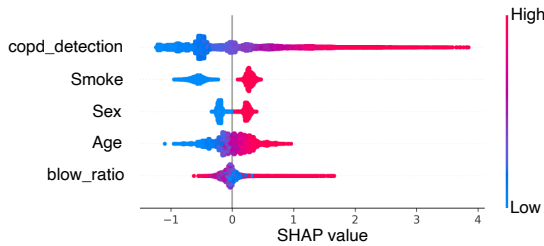


Figure 9: Beeswarm plots. Brighter colors mean that the feature has a more positive impact on the model’s predictions.

As shown in the beeswarm plot in figure 9, the relative importance of features is revealed. The figure shows that the higher the COPD risk value, the greater its impact on the model. Smoking, being male, and older age all influence the model’s judgment. DeepSpiro’s findings are consistent with related research conclusions, indicating that smokers, males, and older patients have a higher risk of being predicted as having COPD.

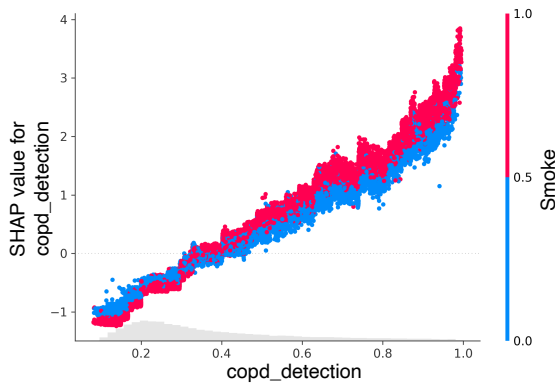


Figure 10: COPD-Detection with smoke.

We examine the relationship between smoking and risk values as well as age and risk values and present our results with dependency graphs. Figure 10 shows the relationship between smoking and the risk of COPD. From the figure, it is evident that the predicted risk value of DeepSpiro is closely related to smoking status. The higher the risk value, the larger the proportion of smokers. This aligns with clinical significance. For COPD patients, smokers are more susceptible to the disease.

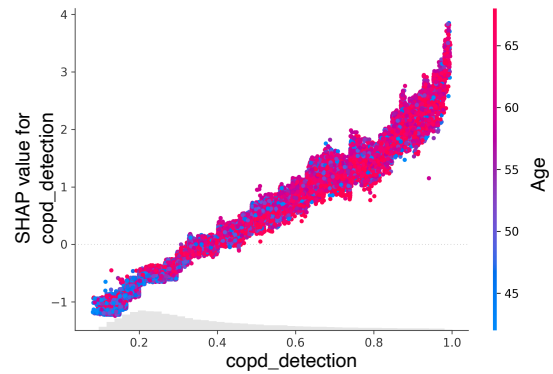


Figure 11: COPD-Detection with age.

Figure 11 illustrates the relationship between age and the risk of COPD. From the figure, it can be seen that the predicted risk value of DeepSpiro is closely related to age. The higher the risk value, the older the age. This aligns with clinical significance. For COPD patients, older patients are more susceptible to the disease.

#### 4.6. Model Explainer Analysis

Healthcare professionals often struggle to accurately identify and locate disease information directly from long sequence data in COPD classification tasks. To address this issue, we utilize SpiroExplainer, automatically focusing on the diseased regions of the Volume-Flow data.

The proposed method can automatically capture anomalies from long sequence Volume-Flow data, providing specific patches with abnormalities. Figure 12 shows that the model can automatically focus on key patches that distinguish COPD patients. Brighter colors indicate higher attention in the corresponding areas, while darker colors indicate lower attention.

An interesting phenomenon is that for non-COPD patients, as shown in Group A of figure 12, the Volume-Flow curve in the  $FEF_{25}$ - $FEF_{50}$  area appears “full,” without the small airway collapse phenomenon near  $FEF_{75}$  at the tail of the curve. DeepSpiro primarily focuses on these two areas near  $FEF_{25}$ - $FEF_{50}$  and  $FEF_{75}$ , which match the characteristics of the non-COPD patient group. On the other hand, for COPD patients, as shown in Group D of figure 12, the curve’s tail near the  $FEF_{75}$  area collapses due to small airway collapse resulting from COPD. DeepSpiro focuses on the area near  $FEF_{75}$ , aligning with the characteristics of the COPD patient group. Thus, DeepSpiro can effectively differentiate and assess the features of different populations.

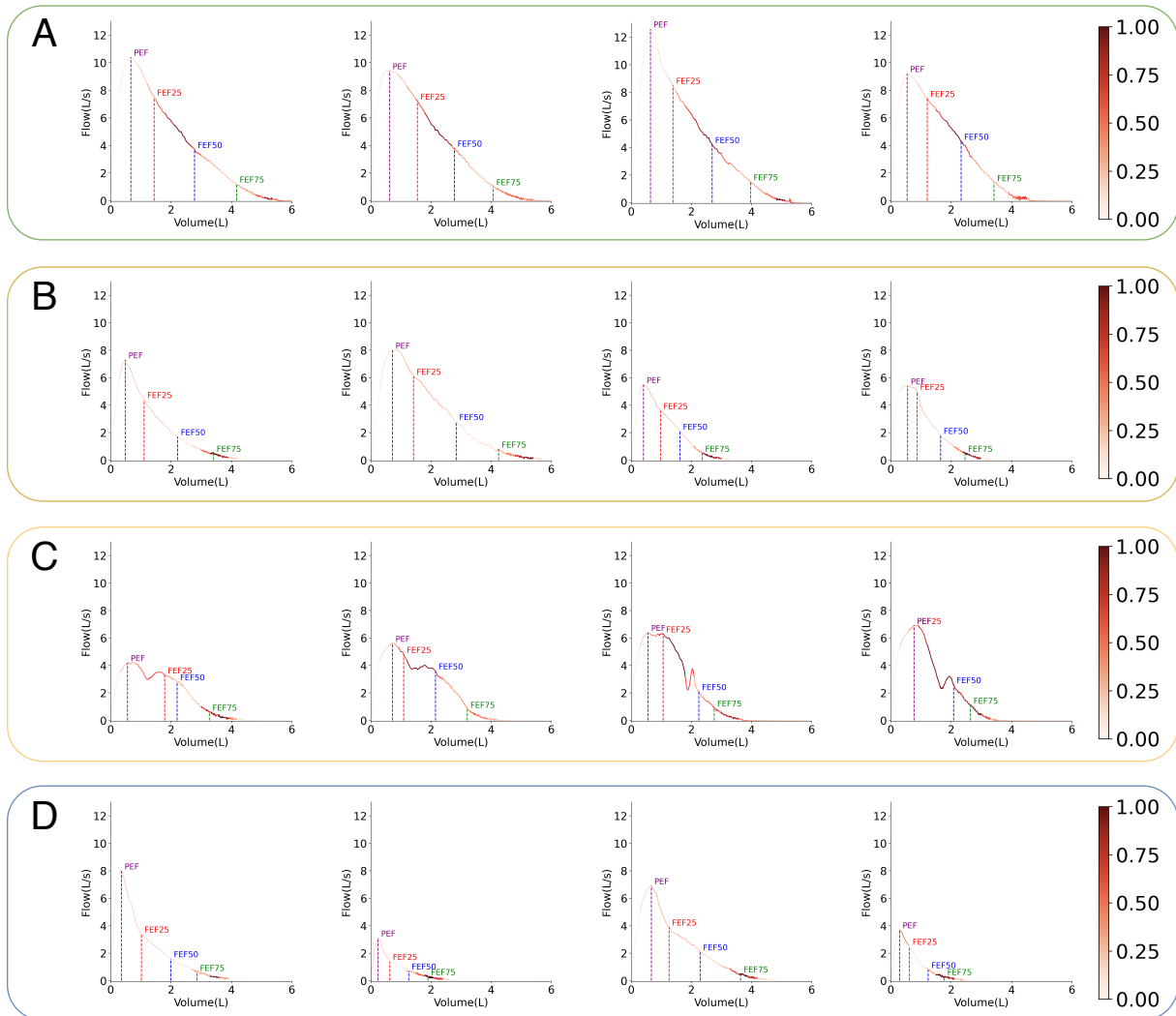


Figure 12: The explainer of the model. The brighter the color, the more attention the model pays. Among them, Group A consists of non-COPD patients detected as non-COPD by the model, Group B consists of non-COPD patients detected as COPD by the model, Group C consists of COPD patients detected as non-COPD by the model, and Group D consists of COPD patients detected as COPD by the model.

In analyzing cases where the model made incorrect predictions, we found that for some individuals who might have asthma, as shown in Group B of figure 12, due to insufficient inhalation, the curve after  $FEF_{75}$  shows a weak exhalation characteristic similar to the small airway collapse seen in COPD patients. Since the model mainly focuses on the area near  $FEF_{75}$ , it leads to lower prediction accuracy for these asthma patients. For some individuals who might have COPD, as shown in Group C of figure 12, due to uneven exhalation effort or mid-breath inhalation by COPD patients, the Volume-Flow curve might present double or multiple peaks, appearing "full" in the  $FEF_{25}$ - $FEF_{50}$  range

similar to non-COPD patients. DeepSpiro primarily focuses on areas near  $FEF_{25}$ - $FEF_{50}$  and  $FEF_{75}$ , which also leads to lower prediction accuracy for these COPD patients. We believe the model's predictions are medically interpretable, and due to the complexity and overlap of disease characteristics, it is challenging to avoid prediction errors completely.

## 5. Conclusion and Future Work

In this paper, we designed a deep learning method for detecting and early predicting chronic obstructive pulmonary disease from the Volume-Flow curve time se-

ries. Specifically, we use SpiroSmoother, thereby enhancing the stability of the Volume-Flow curve. We propose SpiroEncoder, which unifies the temporal representation of "key patches" and achieves the conversion of key physiological information from high to low dimensions. Utilizing SpiroExplainer, we fuse diagnostic probabilities with demographic information to improve the accuracy of COPD risk assessment and the model's explainer. The results and explainer of the model can provide patients with timely COPD risk reports. Moreover, we propose SpiroPredictor, by incorporating key information such as the degree of concavity, the model can accurately predict the future disease probability of high-risk patients who have not yet been diagnosed, thereby enabling early intervention and treatment to slow the progression of the disease.

In the future, we plan to develop user-friendly software tools that allow doctors to conveniently apply the model in clinical settings and obtain reliable and understandable results to assist in diagnosing and treating patients. Finally, we aim to improve the model's generalizability by incorporating more high-quality datasets, enabling it to provide effective predictions in a wider range of scenarios.

## Acknowledgement

Data from the UK Biobank, which is available after the approval of an application at <https://www.ukbiobank.ac.uk>. The authors gratefully acknowledge the financial supports by the National Natural Science Foundation of China under Grant 62202332 and Grant 62102008.

## References

- [1] Jiaying Sun, Ximing Liao, Yusheng Yan, Xin Zhang, Jian Sun, Weixiong Tan, Baiyun Liu, Jiangfen Wu, Qian Guo, Shaoyong Gao, et al. Detection and staging of chronic obstructive pulmonary disease using a computed tomography-based weakly supervised deep learning approach. *European Radiology*, 32(8):5319–5329, 2022.
- [2] Konstantin Willer, Alexander A Fingerle, Wolfgang Noichl, Fabio De Marco, Manuela Frank, Theresa Urban, Rafael Schick, Alex Gustschin, Bernhard Gleich, Julia Herzen, et al. X-ray dark-field chest imaging for detection and quantification of emphysema in patients with chronic obstructive pulmonary disease: a diagnostic accuracy study. *The Lancet Digital Health*, 3(11):e733–e744, 2021.
- [3] Justin Cosentino, Babak Behsaz, Babak Alipanahi, Zachary R McCaw, Davin Hill, Tae-Hwi Schwantes-An, Dongbing Lai, Andrew Carroll, Brian D Hobbs, Michael H Cho, et al. Inference of chronic obstructive pulmonary disease with deep learning on raw spirometry identifies new genetic loci and improves risk models. *Nature Genetics*, pages 1–9, 2023.
- [4] Chenzhong Yin, Mihai Udrescu, Gaurav Gupta, Mingxi Cheng, Andrei Lihu, Lucretia Udrescu, Paul Bogdan, David M Man- nino, and Stefan Mihaicuta. Fractional dynamics foster deep learning of copd stage prediction. *Advanced Science*, 10(12):2203485, 2023.
- [5] Yonghua Zhuang, Fuyong Xing, Debashis Ghosh, Brian D Hobbs, Craig P Hersh, Farnoush Banaei-Kashani, Russell P Bowler, and Katerina Kechris. Deep learning on graphs for multi-omics classification of copd. *Plos one*, 18(4):e0284563, 2023.
- [6] Yanan Wu, Ran Du, Jie Feng, Shouliang Qi, Haowen Pang, Shuyue Xia, and Wei Qian. Deep cnn for copd identification by multi-view snapshot integration of 3d airway tree and lung field. *Biomedical Signal Processing and Control*, 79:104162, 2023.
- [7] Shenda Hong, Yanbo Xu, Alind Khare, Satria Priambada, Kevin Maher, Alaa Aljiffry, Jimeng Sun, and Alexey Tumanov. Holmes: Health online model ensemble serving for deep learning models in intensive care units. In *Proceedings of the 26th ACM SIGKDD International Conference on Knowledge Discovery & Data Mining*, pages 1614–1624, 2020.
- [8] Daiana Stolz, Takudzwa Mkorombindo, Desiree M Schumann, Alvar Agustí, Samuel Y Ash, Mona Bafadhel, Chunxue Bai, James D Chalmers, Gerard J Criner, Shyamali C Dharmage, et al. Towards the elimination of chronic obstructive pulmonary disease: a lancet commission. *The Lancet*, 400(10356):921–972, 2022.
- [9] Alvar Agustí, Bartolome R Celli, Gerard J Criner, David Halpin, Antonio Anzueto, Peter Barnes, Jean Bourbeau, MeiLan K Han, Fernando J Martinez, Maria Montes de Oca, et al. Global initiative for chronic obstructive lung disease 2023 report: Gold executive summary. *American journal of respiratory and critical care medicine*, 207(7):819–837, 2023.
- [10] Shawn D Aaron, Maria Montes de Oca, Bartolome Celli, Surya P Bhatt, Jean Bourbeau, Gerard J Criner, Dawn L De- Meo, David MG Halpin, MeiLan K Han, John R Hurst, et al. Early diagnosis and treatment of copd: The costs and benefits of case-finding. *American Journal of Respiratory and Critical Care Medicine*. (ja), 2024.
- [11] Surya P Bhatt, Arie Nakhmani, Spyridon Fortis, Matthew J Strand, Edwin K Silverman, Frank C Sciruba, and Sandeep Bod- duluri. Fev1/fvc severity stages for chronic obstructive pul- monary disease. *American journal of respiratory and critical care medicine*, 208(6):676–684, 2023.
- [12] Tetsuro Maeda and Mark T Dransfield. Chronic obstructive pul- monary disease and cardiovascular disease: mechanistic links and implications for practice. *Current Opinion in Pulmonary Medicine*, 30(2):141–149, 2024.
- [13] Sepp Hochreiter and Jürgen Schmidhuber. Long short-term memory. *Neural computation*, 9(8):1735–1780, 1997.
- [14] Yunlong Sun, Jingge Lian, Ze Teng, Ziyi Wei, Yi Tang, Liu Yang, Yajuan Gao, Tianfu Wang, Hongfeng Li, Meng Xu, et al. Covid-19 diagnosis based on swin transformer model with de- mographic information fusion and enhanced multi-head atten- tion mechanism. *Expert Systems with Applications*, 243:122805, 2024.
- [15] Anas Abdulalim Alabdullah, Mudassir Iqbal, Muhammad Za- hid, Kaffayatullah Khan, Muhammad Nasir Amin, and Fazal E Jalal. Prediction of rapid chloride penetration resistance of metakaolin based high strength concrete using light gbm and xgboost models by incorporating shap analysis. *Construction and Building Materials*, 345:128296, 2022.
- [16] Md Johir Raihan, Md Al-Masrur Khan, Seong-Hoon Kee, and Abdullah-Al Nahid. Detection of the chronic kidney disease using xgboost classifier and explaining the influence of the at-



- tributes on the model using shap. *Scientific Reports*, 13(1):6263, 2023.
- [17] Xi Wei, Congjun Rao, Xinping Xiao, Lin Chen, and Mark Goh. Risk assessment of cardiovascular disease based on solssa-catboost model. *Expert Systems with Applications*, 219:119648, 2023.
- [18] Zhigang Sun, Guotao Wang, Pengfei Li, Hui Wang, Min Zhang, and Xiaowen Liang. An improved random forest based on the classification accuracy and correlation measurement of decision trees. *Expert Systems with Applications*, 237:121549, 2024.
- [19] Alvaro Fernandez-Quilez. Deep learning in radiology: ethics of data and on the value of algorithm transparency, interpretability and explainability. *AI and Ethics*, 3(1):257–265, 2023.
- [20] Kjell Torén, Linus Schiöler, Anne Lindberg, Anders Andersson, Annelie F Behndig, Göran Bergström, Anders Blomberg, Kenneth Caidahl, Jan E Engvall, Maria J Eriksson, et al. The ratio fev1/fvc and its association to respiratory symptoms—a swedish general population study. *Clinical physiology and functional imaging*, 41(2):181–191, 2021.
- [21] Astri Medbø and Hasse Melbye. Lung function testing in the elderly—can we still use fev1/fvc; 70% as a criterion of copd? *Respiratory medicine*, 101(6):1097–1105, 2007.
- [22] Surya P Bhatt, Pallavi P Balte, Joseph E Schwartz, Patricia A Cassano, David Couper, David R Jacobs, Ravi Kalhan, George T O’Connor, Sachin Yende, Jason L Sanders, et al. Discriminative accuracy of fev1: Fvc thresholds for copd-related hospitalization and mortality. *Jama*, 321(24):2438–2447, 2019.
- [23] Firdaus AA Mohamed Hoessein, Pieter Zanen, and Jan-Willem J Lammers. Lower limit of normal or fev1/fvc; 0.70 in diagnosing copd: an evidence-based review. *Respiratory medicine*, 105(6):907–915, 2011.
- [24] Arka Roy and Udit Satija. A novel melspectrogram snippet representation learning framework for severity detection of chronic obstructive pulmonary diseases. *IEEE Transactions on Instrumentation and Measurement*, 72:1–11, 2023.
- [25] MeiLan K Han, Alvar Agusti, Bartolome R Celli, Gerard J Criner, David MG Halpin, Nicolas Roche, Alberto Papi, Robert A Stockley, Jadwiga Wedzicha, and Claus F Vogelmeier. From gold 0 to pre-copd. *American journal of respiratory and critical care medicine*, 203(4):414–423, 2021.
- [26] Priya Venkatesan. Gold copd report: 2024 update. *The Lancet Respiratory Medicine*, 12(1):15–16, 2024.
- [27] Shireen Mirza, Ryan D Clay, Matthew A Koslow, and Paul D Scanlon. Copd guidelines: a review of the 2018 gold report. In *Mayo Clinic Proceedings*, volume 93, pages 1488–1502. Elsevier, 2018.
- [28] Ting Yang, Renjie Chen, Xiaoying Gu, Jianying Xu, Lan Yang, Jianping Zhao, Xiangyan Zhang, Chunxue Bai, Jian Kang, Pixin Ran, et al. Association of fine particulate matter air pollution and its constituents with lung function: The china pulmonary health study. *Environment International*, 156:106707, 2021.
- [29] Haoyang Hong and Shenda Hong. simplenomo: A python package of making nomograms for visualizable calculation of logistic regression models. *Health Data Science*, 3:0023, 2023.
- [30] Songwei Zhao, Pengjun Wang, Ali Asghar Heidari, Huiling Chen, Hamza Turabieh, Majdi Mafarja, and Chengye Li. Multilevel threshold image segmentation with diffusion association slime mould algorithm and renyi’s entropy for chronic obstructive pulmonary disease. *Computers in Biology and Medicine*, 134:104427, 2021.
- [31] Gabriele Spina, Pierluigi Casale, Paul S Albert, Jennifer Alison, Judith Garcia-Aymerich, Christian F Clarenbach, Richard W Costello, Nidia A Hernandez, Jörg D Leuppi, Rafael Mesquita, et al. Nighttime features derived from topic models for classification of patients with copd. *Computers in Biology and Medicine*, 132:104322, 2021.
- [32] Pooja Sharma, Anuj K Pandey, and Dhruva K Bhattacharyya. Determining crucial genes associated with covid-19 based on copd findings. *Computers in biology and medicine*, 128:104126, 2021.
- [33] Zhifa Han, Huiyuan Hu, Peiran Yang, Baicun Li, Guiyou Liu, Junling Pang, Hongmei Zhao, Jing Wang, and Chen Wang. White blood cell count and chronic obstructive pulmonary disease: A mendelian randomization study. *Computers in Biology and Medicine*, 151:106187, 2022.
- [34] Cries Avian, Muhammad Izzuddin Mahali, Nur Achmad Sulisty Putro, Setya Widyawan Prakosa, and Jenq-Shiou Leu. Fx-net and purenet: Convolutional neural network architecture for discrimination of chronic obstructive pulmonary disease from smokers and healthy subjects through electronic nose signals. *Computers in Biology and Medicine*, 148:105913, 2022.
- [35] Behnood Dianat, Paolo La Torraca, Andreina Manfredi, Giulia Cassone, Caterina Vacchi, Marco Sebastiani, and Fabrizio Pancaldi. Classification of pulmonary sounds through deep learning for the diagnosis of interstitial lung diseases secondary to connective tissue diseases. *Computers in Biology and Medicine*, 160:106928, 2023.
- [36] Yuwei Yang, Yan Cao, Xiaobo Han, Xihui Ma, Rui Li, Rentao Wang, Li Xiao, and Lixin Xie. Revealing exp5 as a potential diagnostic gene biomarker of the late stage of copd based on machine learning analysis. *Computers in Biology and Medicine*, 154:106621, 2023.
- [37] Yubin Lee, Jaeseung Song, Yeonbin Jeong, Eunyoung Choi, Chulwoo Ahn, and Wonhee Jang. Meta-analysis of single-cell rna-sequencing data for depicting the transcriptomic landscape of chronic obstructive pulmonary disease. *Computers in Biology and Medicine*, 167:107685, 2023.
- [38] Ian A Yang, Christine R Jenkins, and Sundeep S Salvi. Chronic obstructive pulmonary disease in never-smokers: risk factors, pathogenesis, and implications for prevention and treatment. *The Lancet Respiratory Medicine*, 10(5):497–511, 2022.
- [39] Mairi MacLeod, Alberto Papi, Marco Contoli, Bianca Beghé, Bartolome R Celli, Jadwiga A Wedzicha, and Leonardo M Fabbri. Chronic obstructive pulmonary disease exacerbation fundamentals: Diagnosis, treatment, prevention and disease impact. *Respirology*, 26(6):532–551, 2021.
- [40] Michael C Ferrera, Wassim W Labaki, and MeiLan K Han. Advances in chronic obstructive pulmonary disease. *Annual review of medicine*, 72:119–134, 2021.
- [41] Majid Mirsadraee, Elnaz Salarifar, and Davood Attaran. Evaluation of superiority of fev1/vc over fev1/fvc for classification of pulmonary disorders. *Journal of Cardio-Thoracic Medicine*, 3(4):355–359, 2015.